Hypotheses in the Life Sciences 1 3 pp 71-84

The Structure of Populations of Budding Yeast in Response to Feedback

Chris C. Stowers[a], Todd R. Young[b] and Erik M. Boczko[c]

a Bioprocess R&D, Dow AgroSciences LLC, Indianapolis, IN 46268
b Dept of Mathematics, Ohio University, Athens, OH 45701
c Dept of Biomedical Informatics Vanderbilt University Medical Center Nashville, TN 37232

Abstract

We describe how the hypothesis of a feedback mechanism involving inter-cellular communication, consistent with known yeast physiological mechanisms, couples growth and division to produce non-stationary, multimodal population densities, that are collected into an integer number of clusters arrayed along the cell cycle. Theoretical analysis and numerical simulations demonstrate that the cell cycle progression of these clusters produces observable oscillation in environmental variables such as dissolved oxygen. We present experimental data and theoretical simulations in support of a model of the periodic population structure that is composed of two clusters.

Corresponding Author

Erik M. Boczko *Dept of Biomedical Informatics Vanderbilt University Medical Center Nashville, TN 37232 Email: erik.boczko@vanderbilt.edu

Introduction

Most laboratory strains of budding yeast, rapidly display equilibrium behaviour when grown in continuous culture. The equilibrium is inferred from the near constant values adopted by such measurable variables as the dissolved oxygen level in the culture media, or the percentage of cells that are budded. However, under some conditions, cultures of yeast do not reach an equilibrium, rather they display periodic oscillations that persist for the duration of the culture.

The periodic oscillation of physiologically relevant variables during the growth and division of a population of budding yeast have been reported and studied for over 40 years [12,18,41,42,59,61,63,66]. The variables that have been observed to oscillate have covered a gamut of biological complexity and include dissolved oxygen, pH, carbon and nitrogen sources such as glucose, ethanol and ammonia, second messengers such as cAMP, the expression level of mRNA's, the activity of metabolic enzymes and indices of growth and division such as the percentage of cells budded and DNA content.

The observed oscillations are of broad interest in biology and chemical engineering for a number of reasons. The control of oscillation and the regulation of yeast metabolism has been an important theme in the chemical engineering literature devoted to the efficient management of bioprocess [9,22,26,55]. The observation of oscillations are also of interest because they expose questions regarding the coordination of the cell cycle and metabolism, and the possible existence of clocks and pacemakers [32,33,34].

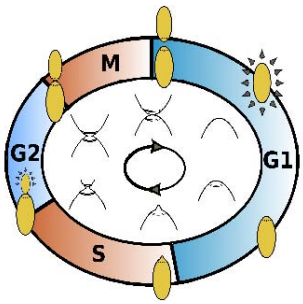

Figure 1: An illustration of the yeast mitotic cell cycle. The cell cycle includes volume growth, budding, DNA replication and cell division. Replication is periodic and often represented as a circle. A more accurate description that includes age stratification is shown in Figure 3.

The existence of autonomous oscillations, as they have been called, and their classification has been investigated and described with regard to intercellular communication [24,45,49].

A majority of the growth conditions reported in the literature produce asynchronously dividing, exponentially growing cultures of budding yeast whose normalized population distribution along a cell cycle coordinate becomes time invariant. Under the assumption of asynchronous, exponential growth, the population structure of a budding yeast culture is described by a continuous population density that declines exponentially with cell cycle position from G_1 to M, and declines geometrically with age [37]. Very little is known about time periodic population structures. Most of the experimental studies that have described population structure have been related to the effort to understand the coordination of yeast volume growth and the sensing mechanisms that gates entry at start [42,65]. The experimental studies of population structure have been limited by the arduous nature of the biophysical characterizations required for which there does not exist any standard, high accuracy methodology [57]. An advantage of theory and computation is that it is straightforward to produce population density profiles as a function of arbitrary variables [54].

1.1 The Maintenance of Synchrony

Cell cycle synchrony in budding yeast has historically been measured from a time series of the percentage of the cells in the population that are budded. Buds emerge at or near the G_1 to S transition and persist until division occurs, see Figure 1. The bud site accumulates chitin that remains as a permanent scar that can be stained to provide a quantitative experimental measure of replicative age. The bud index can be affected in two ways. It can rise as cells become budded and it can decline as budded cells divide and/or as newly divided cells dilute the total population. In a dense and well mixed culture the dilution rate should have no effect on the bud index since removal through dilution is an unbiased linear process. It has been shown that classification error of budded vs unbudded is less than 5% [35].

Strains of budding yeast exhibit an age dependent, volume growth variation that strongly dephases cell cycle synchrony [54,65] under most nutrient conditions and at most dilution rates. Daughter cells are smaller at division than their mothers and consequently have a longer G_1 traverse. Even a small but systematic difference in traverse will eventually lead a culture to desynchronize. Typically no more than three consecutive and damping cycles of bud index synchrony can be achieved [10,62] in the absence of the phenomenon of autonomous oscillation. The maintenance of synchrony in an actively growing culture therefore requires the existence of some mechanism to counteract the natural forces that tend to dephase cell cycle synchrony during growth and division [54]. Similar reasoning appears in slightly different language in [31].

Oscillatory behavior in yeast culture is typically grouped into two or three classes whose designations differ depending on the author [24,49]. A description of the population structure within any of these classes remains an open and fundamental question. It is speculated that the very rapid NADH oscillations produced during anaerobic glycolysis in-vivo could not be observed in the absence of strict population synchrony. It has been demonstrated that acetaldehyde acts as a synchronizing agent in this oscillation [14].

It has been claimed that short period aerobic oscillations in the IFO 0233 strain occur in the absence of mitotic cell cycle synchony. The claim is that metabolic synchony occurs in a culture of yeast cells where the cell cycles of the individual cells are randomized with respect to one another. The literature supporting this claim is reviewed in [46,49], and appears to originate with a single paper [52], that cites a negative result without data.

Several feedback mechanisms have been proposed for the maintenance of cell cycle synchrony. Mechanisms involving metabolite feedback that operate on growth rate are particularly elegant [25]: Oscillating metabolite concentrations produce oscillating growth rates and these can act to locally stabilize synchronous trajectories like a focusing billiard. Based on solid experimental evidence [41,66], it has been suggested [19,41] that during long period aerobic oscillations a burst of glycolysis follows from the liberation of glucose from glycogen and trehalose at the G_1-S boundary. The ethanol produced by the population entering S-phase is proposed to accelerate the growth of cells in G_1. Whether or not this proposition is true, it is an example of positive feedback. In this model an agent secreted by a

proportion of the population in one particular phase of the cell cycle advances the cell cycle progression of those cells earlier in the cycle. In the opposite case of negative feedback, cells would slow or stop their cell cycle progression in response to a secreted factor or metabolite. Again, ethanol has been implicated as a source of delays. For instance, it has been demonstrated that above strain dependent critical concentrations, ethanol slows cell cycle progression [29], and references therein. An extreme example of negative feedback is the response of budding yeast to pheromones such as α-factor, that stop cell cycle progression at the G_1-S boundary. The conclusion is that (nonlocal) feedback is produced by mechanisms involving communication, the end result of which is some degree of population structure.

1.2 Clustering

In [5, 6], we have shown that, more or less generically, feedback models of communication among cells, robustly lead to clustering of cells within the cell cycle. Clustering is defined as the temporal pseudo-synchronization of large sub-populations within the cell cycle. A cluster is a significant group of cells passing through cell-cycle milestones, such as budding or division, at nearly the same time. A cluster is akin to a group of runners, close together with respect to the total length of the track, and moving together with comparable speed. A single cluster would represent total population synchrony and would produce a unimodal, periodic, population distribution. Multiple clusters represent a state between total population synchrony and uniform asynchrony.

That positive or negative feedback can cause spontaneous polarization in subpopulations was already appreciated by Muller et al. [41] in their work on the dynamics of population structure, and on a theoretical level by Rotenberg [50] who considered externally applied periodic negative feedback at cell division and demonstrated numerically that clustering occurs in the model. Clustering has also been hypothesized to result from feedback of a form different than what we have considered [67]. It is also well recognized that feedback can produce synchrony in physical and biological systems and has been extensively studied [1,2,3,17,20,21,30,36,39,40,47,51,56,58] (and by many others). A key observation from the mathematical models is that positive feedback typically leads to synchrony, while negative feedback systems tend to clustering[6].

We have considered several realizations of cell-cycle communication models [5,6] supposing only that the appearance of a thresholded population of cells in one interval of the cell cycle, denoted as S, effects the growth of cells in another interval, called R, see Figure 2. That is, if the integrated population density in the S interval is larger than some threshold T, then the cells in the R interval are either advanced or delayed depending on the operative feedback mechanism. We have chosen the label S in analogy with the hydrogen sulfide evolution models of short term oscillatory control [43, 64] and the label R, for responsive. Despite its naturality and potential widespread usage in quorum sensing systems [23] models with non-local coupling of the feedback are not yet fully understood.

The specific number of clusters that form depends on the widths of the S and R intervals, and not on the form of the feedback. If clustering occurs, then there are an integer number of clusters.

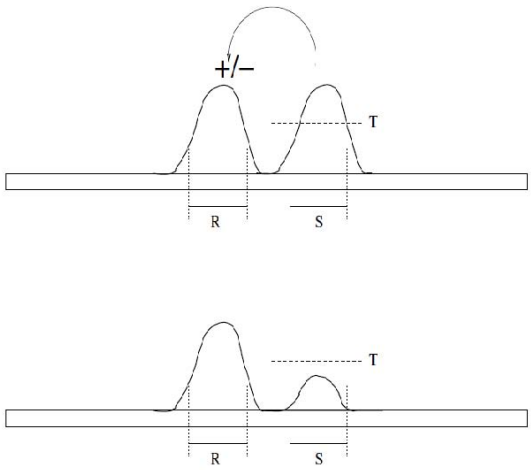

Figure 2: Schematic representation of the density dependent, non local, feedback models that we have been exploring mathematically [5,6]. The horizontal axis represents the cell cycle from G_1 on the left to M on the right. The vertical axis represents population density. When the cells in the signaling interval, denoted S are at or above the threshold T, the cells in the responsive interval, R, experience either positive or negative feedback that increases or decreases the rate at which they are progressing through the cell cycle.

This explains the periodic-looking behaviors seen in autonomous oscillations. It can be shown that not only are the number of clusters bounded above, but in certain circumstances, also bounded below, meaning that clusters must form. Feedback models achieve clustering even in the presence of small random perturbations.

Table 1: Mineral Solution A

Salt	Concentration
FeSO4 • 7H2O	40gm/L
ZnSO4 • 7H2O	20gm/L
CuSO4 • 5H2O	10gm/L
MnCl2 • 4H2O	2gm/L
75% H2 SO4	20mL/L

2 Material and Methods

2.1 Experiments

Continuous Culture.

The haploid strain CEN.PK 113-7D(mat a) of budding yeast were cultivated in 3L New Brunswick Scientific Bioflow 110 reactor equipped with two Rushton type impellers, operated at 550 rpm. Air was sparged at a rate of 900 mL/min. Temperature was maintained at 30 degrees Celsius and pH was automatically controlled with 2 N sodium hydroxide.

Overnight cultures were grown in YPD media with shaking. 20mL were inoculated into a reactor containing 850 mL of synthetic media with the following composition: 10gm per liter anhydrous glucose (SigmaG71528), 5gm per liter ammonium sulphate (SigmaA2939), 0.5gm per liter magnesium sulfate heptahydrate (Sigma M2773), 1 gm per liter of Yeast Extract (Becton, Dickinson and Company Cat288620),2gm per liter potassium phosphate (SigmaP5379), 0.5 mL per liter of 70% v/v sulfuric acid, 0.5 mL per liter of antifoam A (Sigma 10794), 0.5 mL per liter of 250 mM calcium chloride, and 0.5 mL per liter of mineral solution A, see Table 1.

The culture was subsequently grown in batch mode for 12-16 hours until it reached a cell density of approximately $5 \cdot 10^9$ cells/mL. Continuous culture ensued with a dilution rate of 0.088 per hour. Samples were taken from the reactor and flash frozen using dry ice.

Measurement of Bud Index and Cell Density

Cell samples were thawed in a 4C sonicating water bath for 5 minutes and vortexed briefly. One μL of sample was resuspended in 10mL of Isoton Diluent (Sigma) and vortexed. The cell density of three independent half mL samples were measured using a Beckman Multisizer Coulter counter. The sizing threshold was 2-8μm.

Samples were stained with1 mg/ml Primulin [48] for5 minutes at room temperature, washed and resuspended in PBS. Bud scars were counted using a conventional Nikon TE-2000 microscope with a 100X objective and a DAPI fluorescence filter. No less than 100 cells were scored per frame. A minimum of three independent frames were scored per time point. The 0

Table 2: Age distribution data for CENPK growth during autonomous oscillation. The generational doubling times, T_k, calculated from the age distribution are also shown.

Generation	Fraction	T_k
0	0.5491	8.8
1	0.2407	8.2
2	0.1098	7.6
3	0.537	7.2
4+	0.0467	_

bud index was scored under white light from the same frame of cells used to count scars.

2.2 Modeling

Leslie Model Simulations

At the greatest level of detail we have considered models of budding yeast growth and division that are parameterized with experimental data and that are stratified with respect to cell cycle progression and age, see Figure 3. The data used to parameterize the model include age class dependent growth milestones such as the average size of a cell at bud emergence and the

variance in that value. Such data are available in the literature for some strains [65], and we have made measurements for others. We have shown that these models can capture the complexity of yeast growth dynamics and account for strain variations therein [54,55]. The oxygen consumption of the population, as shown in Figure 7, is calculated by taking the inner product of the population distribution as a function of the cell cycle, with the single cell profile shown in Figure 4.

3 Results

3.1 Existence of Clusters

Figure 5 shows three experimental time series collected over a 412 minute time period. The time series correspond to the dissolved oxygen trace, bud index oscillation and the cell density data. Two dissolved oxygen oscillations occur within the time period that corresponds to the doubling time of the dilution rate set in the experiment. Over the course of an oscillation the bud index percentage falls below 8%, and in a time span of 80 minutes rises to nearly 50%.

The fact that the bud index reaches nearly 50% and that this occurs twice within the culture doubling time shows that nearly half of the cells enter S-phase as a cluster, while the other half remain unbudded and reside in *G1*. In the subsequent oscillation, the other half of the population density enters S-phase again as a cluster. The population density is organized into two clusters. Furthermore the data delimit two asymmetric phases within each oscillation, that naturally define both a symbol sequence and model of the population structure, see Figures 6 and 9.

The relationship of the density data to the bud index data is extremely informative. We draw the following conclusions. First, as the bud index rises to its maximum the cell density is purely in decline. From the slope of this decline we calculate a dilution rate that is within less that 8% error of the dilution rate set in the experiment, see also Figure 10. This is well within the deviation and statistical noise of the measurements and is strong evidence that no cell division is taking place as a cluster passes into the S-phase. The subsequent drop in bud index from its maximum value corresponds to a rise in cell density, indicating that loss of buds is due to cell division of that cluster.

Second, the relation between the cell density maximum and the subsequent bud index minimum,

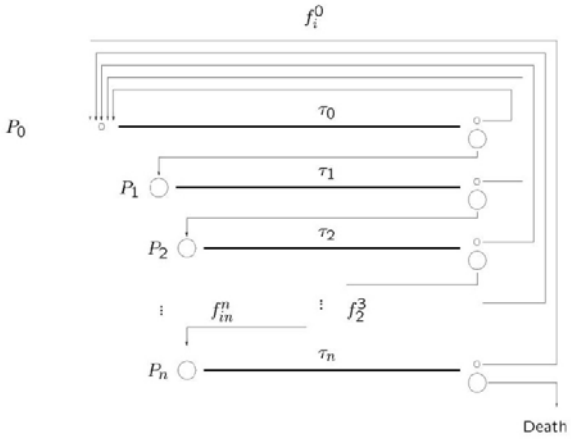

Figure 3: The growth and division of a population of yeast stratified by cell cycle position and age. The horizontal axis represents cell cycle position from G1 on the left to M on the right. Replicative age increases from the daughter, P0, age class downward along the vertical axis. This is the schema that we have used in the Leslie model simulations described in the text. The symbol $f_{in}^i(t)$ is the total flux of cells entering the ith generation at time t. The quantities, $f_i^0(t)$, are the total number in (t) of daughter cells produced from a division in age class i at time t. The values of the flux residence times, Tk, are determined from experiment, see for instance Table 2, and describe the generational doubling times and length of the individual, age class dependent, cell cycles.

indicate that there exists a short period of time when both clusters coexists in the *G1* phase.

Given the sampling rate, we can estimate this time to be on the order of 15 minutes. The magnitude of the bud index minimum, approximately 8%, is further indication of this temporal coexistence. The phase relation between these events represents the timing and spacing between the cell clusters, such that as the tail of the dividing cluster is passing through M-phase and all of its cells are returning to a *G1* phase, the second cluster's leading edge is passing into the *S*-phase and is beginning to bud.

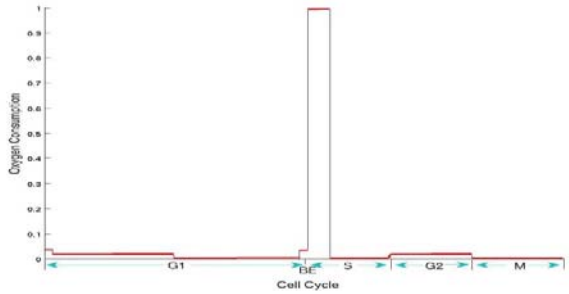

Figure 4: Single cell oxygen consumption profile used in the model simulations of yeast growth and division. The figure indicates how oxygen is consumed by the cell over the cell cycle. The result of using this profile is shown in Figure 7.

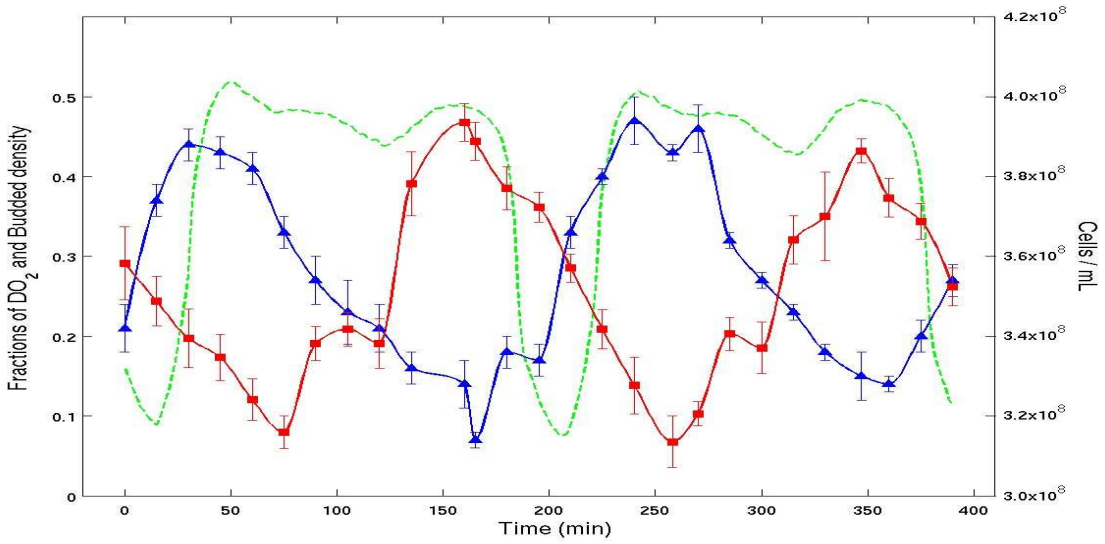

Figure 5: Experimentally measured dissolved O_2 (greendashed), bud index (blue triangles) and total cell number (red squares) oscillations as a function of time during CENPK autonomous oscillation. Two oscillations occur within the approximate dilution rate doubling time of 6.86 hours. Error bars represent a standard deviation determined from triplicate repeats.

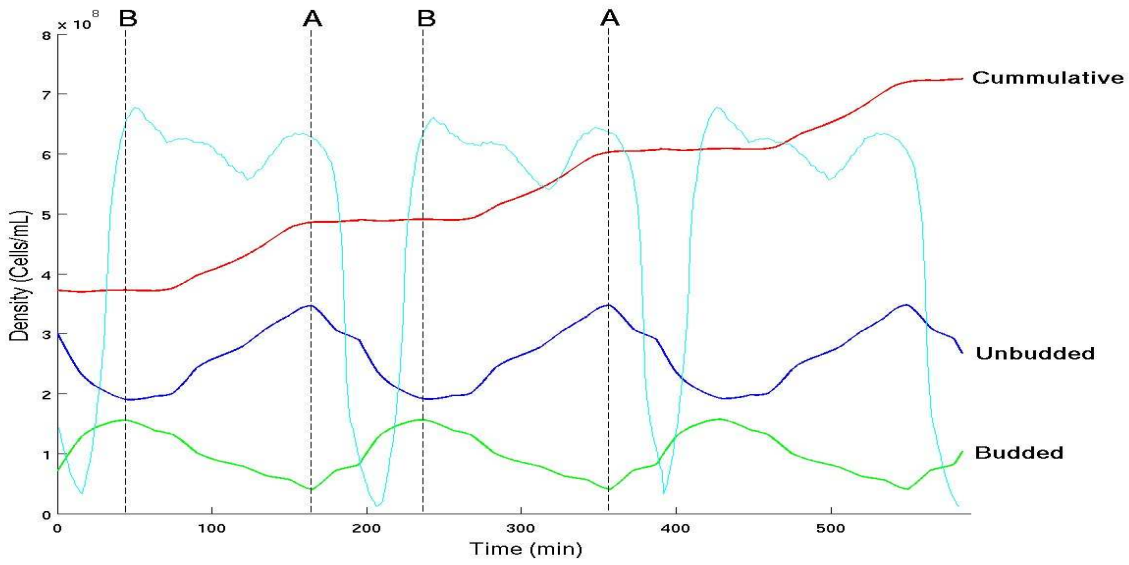

Figure 6: Cumulative cell density, budded and unbudded cell density as function of time for the experimental time series data shown in Figure 5. Two phases, a post-replicative phase A, and a pre-replicative phase B, are indicated by the dashed lines. It is observed that the A to B transition is shorter than the replicative transition B to A. The features of the density data clearly and naturally identify these periodic states and their transitions. The transitions between states correlate perfectly with those of the dissolved oxygen profile.

Third, the close temporal interplay between the bud index minimum and the cell density maximum contains more information. The cells at the density max must be in early G_1. These same cells cannot begin to bud within the next fifteen minutes. The cells at the bud index minimum are doing just that. This indicates the existence of multiple clusters of cells. The fact that two oscillations occur within one dilution rate doubling time testifies to the interleaving of two clusters.

The temporal width of the bud index curve from its global maximum to the following global minimum indicates the width of the group of daughter cells that emerge within the *P0* generation due to the cell divisions.

The temporal width is 115 minutes, Figure 5. The temporal distance from the bud index minimum to the following global maximum represents an upper bound on the time it takes the a cluster to pass into *S*-phase, and this time is 80 minutes. If the clusters are moving through the cell cycle at uniform speed then the differences in these times reflect a narrowing of the daughter part of the cluster as it passes through G_1. There are several conceivable mechanisms that could effect this change. Since all cells do not bud at precisely the same cell cycle position or volume, the simultaneity induced by the dispersion in the budding process could account for some or all of the effect. We believe that this narrowing is at least in part an indication of the feedback mechanism that produces the clustered population structure by reducing the temporal variance within the daughter population by 55-70% over the course of its G_1 traverse. While dilution will progressively whittle away at a cluster of cells throughout their cell cycle traverse, it cannot theoretically alter the width of the cluster at half-height. More data are required to further sharpen these deductions.

The symmetry of the bud index and cell density curves contain meaning. The fall in the bud index is not as sharp as its rise. Simulations indicate that the trailing tail is due to the fact that the different age classes do not divide in unison. This is supported by the fact that the cell density appears to have three distinct peaks, a fact also seen in simulations. This is also supported by generational doubling times calculated from the experimental age distribution data, see Table 2, that suggest that the length of the parent cell cycles become

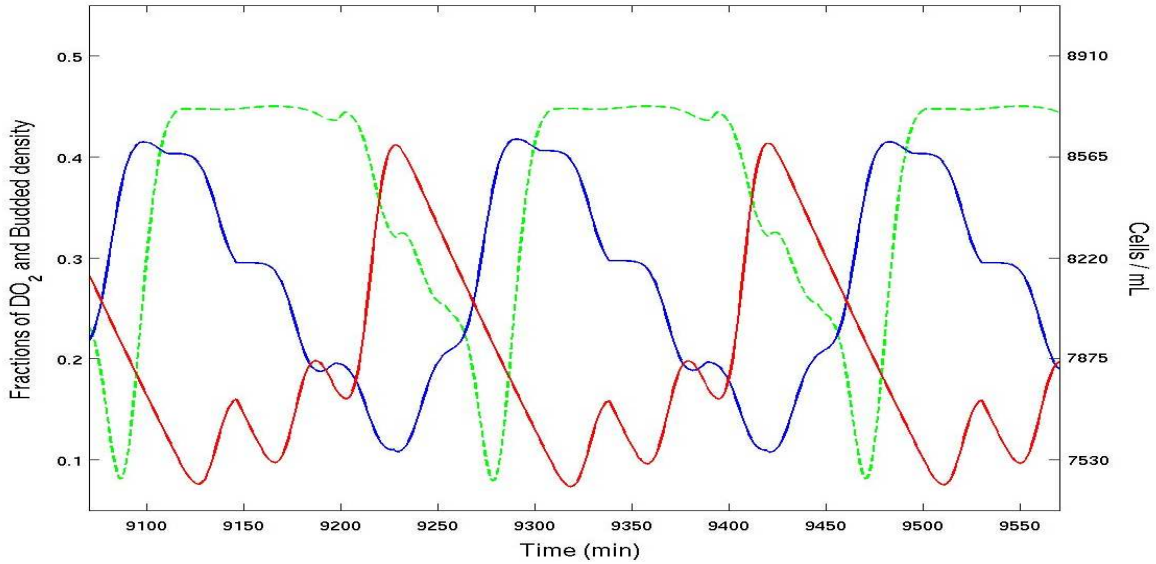

Figure 7: Dissolved O_2 (green dashed), bud index (blue) and total cell number(red) oscillations as a function of time from a model simulation with a negative feedback mechanism, see Figure 3. The simulation results recapitulate the observed experimental data seen in Figure 5.

progressively shorter. Another observation is that the sharp rise in the bud index curve to its maximum could be indicative of a blocking mechanism near the *G1*-*S* boundary. A blocking mechanism would cause cells to pile up along the leading edge of a cluster, while leaving a trailing tail, as observed.

3.2 Description of the Population Structure

From the data we can construct a description of the population structure and its dynamics. At the low point of the bud index one cluster of newly divided cells from the previous trailing tail are entering the early *G1* phase. Simultaneously the second cluster is leaving *G1* and entering the *S*-phase in the consecutive bud index upswing. The cluster entering *S*-phase is highly coherent relative to the length of the cell cycle. The sharp rise in the bud index indicates that the cluster has a fairly sharp leading edge. This state of the system is clearly identifiable from the data and in Figure 9 we have labeled this the *A*-state.

We consistently imagine cell cycle traverse from left to right. As the rightmost cluster buds the bud index rises and there is no accompanying rise in cell number. The budding transition lasts 80 minutes and ends in the B-state that is characterized by the bud index maximum. The following transition from the B-state back to the A-state is accompanied by cell division and is the longer of the two transitions.

As the bud index declines from its maximum value the long tail indicates a loss of coherence. This is either due to dispersion in the division times of individual cells or the staggered division of different age classes due to variations in the lengths of their cell cycles or a combination of both. The experimental age distribution data and an analysis of model simulations suggest that the tail results from the staggered division of different age classes due to variations in the lengths of their cell cycles. Over the following 115 minutes the rightmost cluster must undergo division since that is the only way to leave the budded state.

During this time period the other half of the cells began and ended in the unbudded state, that must be *G1*, and therefore that cluster of cells must have been in *G1* during the whole period. The next rise in bud index level can only be ascribed to these cells since the cells in the first cluster have clearly not had time to pass all the way through the *G1* phase and bud again.

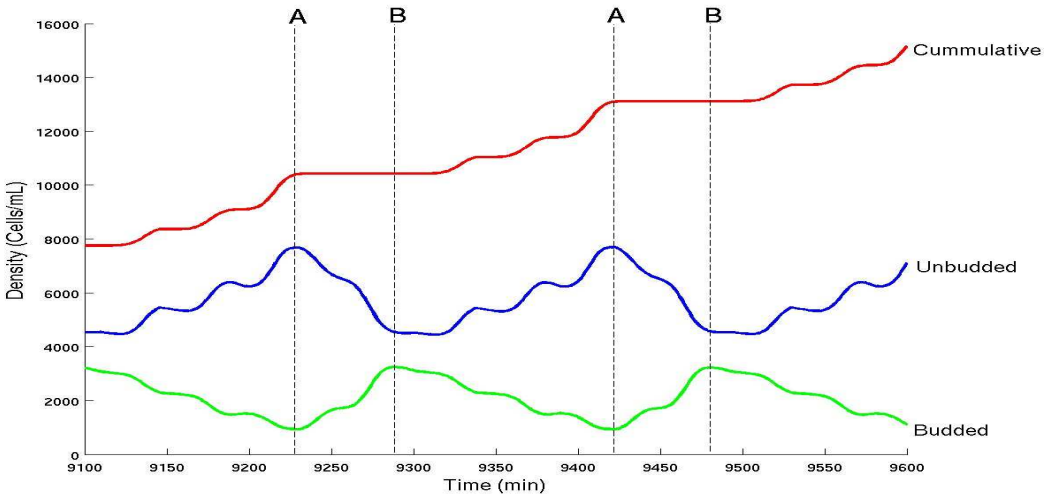

Figure 8: Cumulative cell density, budded and unbudded cell density as function of time for the simulation data shown in Figure 7. Two phases, a post-replicative phase A, and a pre-replicative phase B, are indicated by the dashed lines. It is observed that the A to B transition is shorter than the replicative transition B to A. The key difference between the simulation results and the corresponding experimental results shown in Figure 6 is that the simulation shows in greater detail small variations in density that arise from older generations.

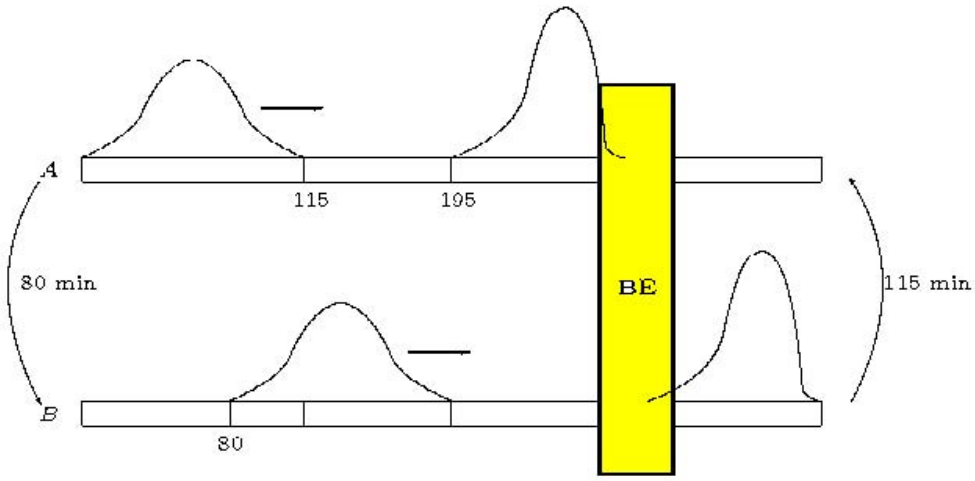

Figure 9: A model of the two phases of an oscillation that is consistent with all experimental and theoretical data. The timings reflect the details gleaned from the experimental time series data shown in Figure (5) and Figure (6). The horizontal axis represents cell cycle progression from G_1 on the right, to the end of *M* at the extreme left. The vertical axis represents population density. Two snaphots of the population dynamics are shown. The *A* state emerges after cell division with nearly all the cells in G_1. The rightmost cluster passes into the *S*-phase over the next 80 minutes as the *A* state passes into the *B* state. The G_1 -*S* boundary lies within the yellow band labeled as bud emergence (*BE*). The rightmost cluster of cells divides as the *B* state returns to the A state, the previously leftmost cluster having reached the G_1-*S*-phase boundary. The course grained system exhibits period oscillation of the two states ABAB..., indefinitely.

The second group of cells then enters S-phase as a strongly coherent cluster in the same way as the previous one. This leaves only a description of what happens to the cells during G_1. From the tiered decline in bud index level described above, a broad cell cluster enters G_1. Apparently as the cells pass through G_1, coherence is restored, resulting in a fairly tight cluster of cells that enter *S*-phase again.

3.3 Factors Consistent with Clustering

We present two lines of evidence that further support the hypothesis that the population structure is composed of two clusters of cells. First, from experimental age distribution data, and also from the combination of bud index and the cell density data, we have estimated the average lengths of the cell cycles of the different age classes. Second, by integrating the cell density data we can determine the relative increase in density per oscillation. A simplified analysis shows that the relative increase depends on the number of clusters in a predictable way. The data are consistent with two clusters.

The hypothesis of 2 cell clusters, as described in the previous section, is consistent only with cell-cycle lengths that are either nearly the same over the first few generations, or if the daughter cell cycle is approximately twice as long as that of the parents. If it were otherwise a cluster would become incoherent at cell division, because generations with significantly shorter cell cycles would "get ahead" of its cluster. With more than 2 clusters, this problem could be remedied by the cells in the faster generation falling roughly into another temporally advanced cluster. For instance if parent generations had cell cycle lengths which were roughly 2/3 of the cycle length for daughter, then 3 clusters could be supported. Or, if the ratio was 3/4 then 4 clusters could be supported.

Independent of the relationship between the lengths of the cell cycles of the individual age classes, the partitioning of the cell cycle phases, specifically the G_1-*S*-phase boundary, impacts the population dynamics. For the above description to be valid, it must be the case that cells spend more than half of their time in the G_1 phase. Otherwise, the two or more cluster picture, or any more dispersed profile, could not result in a bud index oscillation from nearly 0% to 50%. It has long been appreciated that metabolic alterations in cell cycle length prolong or contract G_1 [53]. Our modeling hypothesis of positive or negative feedback are tacitly assumed to impact cells during their G_1 traverse. An analysis of the time-series data shown in Figure 5 indicates that there are two distinct phases to each oscillation. These phases can be distinguished from the data as a division phase, that we label by the transition $B \rightarrow A$, and a budding phase that we label by the transition $A \rightarrow B$. The state A corresponds to the bud index minimum just prior to the dissolved oxygen minimum and the state B corresponds to the bud index maximum. The dynamic iteration of these states is envisioned in Figure 9, a pair of transitions mark each oscillation and four transitions fill a single dilution doubling time. The $A \rightarrow B$ transition is the shorter of the two.

The data suggest a model in which the cells spend roughly 65% of the time in G_1. The time average bud index, Q, calculated from the experimental data is roughly27-28%. Given that the population density is periodic it can be shown that the time average density remains proportional to $\exp(-Dt)$, where D is the dilution rate, $DP = \ln(2)$, and t represents cell cycle position. Given this representation of the average population density, the estimated average time of bud emergence relative to the average cycle time is given by the formula: $\frac{t_b}{P} = \frac{\ln\left(\frac{1}{1+Q}\right)}{\ln(2)}$. These data and calculations indicate that, on average, bud emergence takes place 267 minutes into the 412 minute cycle shown in Figure 5.

In [4] an algorithm is derived to find the lengths of the cell cycles of the various generations from age distribution data. In Table 2 the first column is the replicative age and the second is the fraction found of that generation in the population. The third column is the length of cell cycles for each generation calculated from the age distribution using the algorithm of [4]. The known dilution rate doubling time is assumed in the calculation. If the τ_k values were equal across all generations, k, then the age distribution at steady state would be exactly geometric with $r = 0.50$, i.e. each generation should be half as numerous as the generation preceding it. For the measured age

Figure 10: The cumulative density time series corresponding to the CENPK autonomous oscillation data shown in Figure 5 in red. The cumulative density increases in 31.5% fractions of the total. This is consistent with a synchronous system having two cell clusters as depicted Figure 9. The analysis behind this conclusion is described in the text.

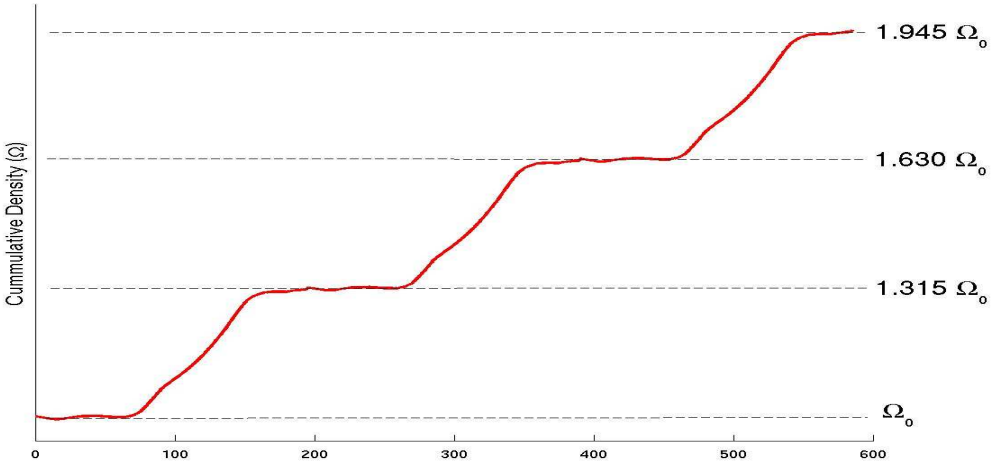

distribution we find almost exactly a geometric progression, but with r =0.46. The values of τ calculated from the data indicate that the discrepancy of timespan between the daughter and first parent generations is about 0.6 hours or a percentage difference of 7%. These two generations together account for 79% of the total density. Simulations based on the derived cycle times and a blocking mechanism is able to reproduce the experimental data, see Figure 7.

Any system with a periodic, multimodal, population density cannot double within a dilution rate, D, doubling time: P, with DP = ln(2). This is because in such a system the total population density must oscillate and during some periods of time little or no population divisions occur. During these times, dilution prevails. Let $T_n(t)$ represent the total population density of an idealized system with n synchronous clusters. The variable t can be thought of as time or position in the cell cycle. Then the function $F_n(z) := T_n(z) + D\int_0^z T_n(x)dx$ represents the accumulated density adjusted for effluent loss due to dilution (with dilution rate D). Consider what happens to the density profile, $T_\infty(x) = Ke^{-Dx}$, that corresponds to asynchronous growth. In this case the accumulated density F_∞ will double exactly in one period P. In contrast, calculations of the behavior of the function F_n based on idealized synchronous systems indicate that systems with n humps will jump in density in fractions of the total that depend on $n: \left(1 - e^{-D/n}\right)$. For two clusters the system jumps 29% of the total with each hump, and requires three oscillations to double. A system with three clusters is expected to jump only 20% per hump, and require roughly five oscillations to double. An analysis of our experimental data, indicates that the total density increases 31.5% per oscillation, see Figure 10. This is fully consistent with two clusters of cells.

Discussion

Mathematical modeling, analysis and simulation show that threshold triggered feedback mechanisms can initiate clustering over a wide range of parameter values and initial conditions. The conclusion is that clustering is a robust phenomenon that could arise from quorum sensing.

The Bud index data along with the cell density data in the CEN.PK strain show conclusively that clustering occurs. The experimental evidence presented in Figure 5 supports the conclusion that two independent critical clusters exist each containing roughly half the total cells. Further, the clustering of the population density

and its subsequent cell cycle progression accounts for the observed O_2 oscillations.

The Leslie model simulations of a negative feedback model shown in Figures 7 and 8, agree both qualitatively and quantitatively with the corresponding experimental data shown in Figures 5 and 6. The simulations provide a prediction of the dynamic progression of the clusters and a detailed picture that is instructive to interpret experimental results and to design experiments that progressively reveal the finer structure and coordination between metabolism, communication and clustering.

What remains unresolved are the specific details of the feedback mechanism that entrains the cells. While the role of oxygen in quorum sensing has been clearly established [7], and interesting hypothesis have been advanced for why it might act in that capacity in the CEN.PK oscillations [12,59], its position in the hierarchy of cause and effect has not yet been convincingly elucidated in autonomous oscillations. There exist interesting and related cautionary physiological tales involving ostensibly oxygen driven processes [16]. It is likely that multiple agents are involved.

Our hypothesis, consistent with the data is that the cell cluster that is approaching the G_1-S boundary, in the A-state, is secreting a synchronizing agent that acts on the newly emerged cluster in early G_1. It is not clear if the feedback is only sensed by daughter cells or by cells in G_1 of all ages. It is possible that cohesion established among daughter cells is maintained well enough with age that the system as a whole remains cohesive, coupled with the fact that successive generations decay in population density geometrically. The fact that the population structure is robustly altered by pH in a way that is qualitatively different from dilution indicates that communication is involved[9].

While our aim is to understand the population structure, we remark in conclusion on the connection between the population dynamics and the metabolic dynamics encoded in the dissolved oxygen oscillation. The data shown in Figure 6 clearly indicate that the utilization of dissolved oxygen occurs during the A to B transition. The *B to A* transition is marked by cell division. The data are consistent with G_1 phase oxidative metabolism and the supposed bonfire of storage carbohydrates that precedes start in slowly growing aerobic cultures [19,41,42,66]. Since G_1 is the only phase without buds, the bud index minima and cell density maximum indicate that from 85-95% of the cells are in G_1 prior to the large downswing in dissolved oxygen. The minimum in the bud index occurs as a cohort of newly divided cells appear as a uniform cluster in the G_1 phase. At the same time the leading edge of the second cluster reaches bud emergence. At the dissolved oxygen minimum, slightly more than half the cluster has budded and the cell density profile shows only loss due to dilution, indicating that most all cell division has ceased.

Acknowledgment

The authors dedicate this work to the memory of Robert Klevecz. This work was partially supported by NIHRO1GM090207.

References

[1].Antoneli F, Dias AP, Golubitsky M, Wang Y, (2005) Patterns of synchrony in lattice dynamical systems. Nonlinearity 18:2193–2209.

[2].Aston PJ, Bird CM,(1998) Synchronization of coupled systems via parameter perturbations. *Phys. Rev.* E 57:2787-2794.

[3].Balmforth, NJ, Sassi R, (2000) A shocking display of synchrony. Bifurcations, patterns and symmetry. *Phys. D* 143:21-55.

[4].Ban H, Boczko EM (2008) Age distribution formulas for budding yeast. Vanderbilt University e-archive Technical Report available at http://hdl.handle.net/1803/1166.

[5].E.M. Boczko, C. Stowers, T. Gedeon and T.Young (2009) ODE, RDE and SDE models of cell cycle dynamics and clustering in yeast. *J. Biological Dynamics* 4:328-345. (NIHMS147352)

[6].T.R. Young, B. Fernandez, R. Buckalew, G. Moses, E.M. Boczko (2012)Clustering in cell cycle dynamics with general response/signaling feedback. *J. Theor. Biol*. 292:103-115.

[7].Bose JL, Kim U, Bartowski W, Gunsalus GP, Overlay AM, et al.(2007) Bioluminescence in Vibrio fisheri is controlled by the redox-responsive regulator *ArcA. Mol. Microbiol.* 65:538-553.

[8].Boye E, Stokke T, Kleckner N, Skarstad K (1996) Coordinating DNA replication initiation with cell growth: Differential roles for Dna A and Seq A proteins. *Proc. Natl. Acad*. Sci. 93:12206-12211.

[9].Buese M, Kopmann A, Diekmann H, Thoma M(1998) Oxygen, pH value, and carbon source induced changes of the mode of oscillation in synchronous continuous culture of Saccharomyces cervisiae. Biotechno. Bioeng. 63:410-417.

[10].Breeden LL (1997) α-Factor synchronization of budding yeast. *Methods in Enzymology* 283:332-342.
[11].Chen H, Fujita M, Feng Q, Clardy J, Fink GR (2004) Tyrosol is a quorum sensing molecule in Candida albicans. *Proc. Natl. Acad*. Sci. 101:5048-5052.
[12].Chen Z, Odstrcil EA, Tu BP, McKnight SL(2007) Restriction of DNA replication to the reductive phase of the metabolic cycle protects genome integrity. *Science* 316:1916-1919.
[13].Collier J, McAdams HH, Shapiro L (2007) ADNA methylation ratchet governs cell cycle progression through a bacterial cell cycle. *Proc. Natl. Acad. Sci*. 104:17111-17116.
[14].Dano S, Sorensen PG, Hynne F (1999) Sustained oscillations in living cells. Nature 402:320-322.
[15].Dunny GM, Leonard BAB (1997) Cell cell communication in Gram Positive bacteria. *Annu. Rev. Microbiol*. 51:527-564.
[16].Edwards JC, Johnson MS, Taylor BL (2006) Differentiation between electron transport and sensing and proton motive force sensing by the Aer and Tsr receptors for aerotaxis. *Mol. Microbiol*. 62:823-837.
[17].Ermentrout B, (1991) An adaptive model for synchrony in the firefly Pteroptyxmalaccae. J. Math. Biol. 29: 571-585.
[18].Finn RK, Wilson RE (1954) Population dynamic behavior of the Chemostat system. *Agric. Food Chem*. 2:66-69.
[19].Futcher B (2006) Metabolic cycle, cell cycle and the finishing kick to start. *Genome Biology* 7:107-111.
[20].Gage TB, Williams FM, Horton JB, (1984) Division synchrony and the dynamics of microbial populations: a size-specific model. *Theoret. Population Biol.* 26:296–314.
[21].Hale JK, (1998)Synchronization by diffusive coupling. Proceedings of Topological Methods in Differential Equations and Dynamical Systems (Krakw-Przegorzay,1996).*Univ.Iagel. Acta Math.* 36:17-31.
[22].Heinzle E, Dunn IJ, Furakawa K, Tanner RD(1982) Modeling of sustained oscillations observed in continuous culture of Saccharomyces Cerevisiae. in Modeling and control of biotechnical processes 1st IFAC Workshop:57-65.
[23].Hense BA, Kuttler C, Muller J, Rothballer M, Hartmann A, Kreft J(2007) Does efficiency sensing unify diffusion and quorum sensing? *Nat. Rev. Microbiol*. 5:230-239.
[24].Henson MA (2005) Cell ensemble modeling of metabolic oscillations in continuous yeast cultures. *Comput. Chem. Enginer*. 29:645-661.
[25].Hjortsø MA, Nielsen J (1994)A conceptual model of autonomous oscillations in microbial cultures. *Chemical Engineering Science*, 49:1083-1095.
[26].Hjortsø MA (1996) Population balance models of autonomous periodic dynamicsin microbial cultures. Their use in process optimization. *Can. J. Chem. Engin*., 74:612-620.
[27].Hornby JM, Jensen EC, Lisec AC, Tasto JJ, Jahnke B, et al. (2001)Quorum sensing in the dimorphic fungus Candida albacans is mediated by farnesol. *Appl. Environ. Microbiol*. 67:2982-2992.
[28].Jones KD, Kompala DS (1999) Cybernetic model of the growth dynamics of Saccharomyces cervisiae in batch and continuous culture. *J. Biotechnol*. 71:105-131.
[29].Jones RP (1989) Biological principles for the effects of ethanol. *Enzyme Microb. Technol*. 11:130-153.
[30].[30] Karbowski J, Ermentrout GB, (2002) Synchrony arising from a balanced synapticplasticity in a network of heterogeneous neural oscillators. *Phys. Rev*. E 65:031902
[31].Keulers M, Satroutdinov AD, Sazuki T, Kuriyama H (1996) Synchronization affector of autonomous short period sustained oscillation of Saccharomyces cerevisiae. *Yeast* 12:673 682.
[32].Klevecz RR (1976) Quantized generation time in mammalian cells as an expression of the cellular clock. *Proc. Natl. Acad. Sci*. 73:4012-4016.
[33].Klevecz RR, Kaufman SA, and Shymko RM (1984) Cellular clocks and oscillators. Inter. Rev. Cytol. 86:97-128.
[34].Klevecz RR, Murray D (2001) Genome wide oscillations in expression. *Molecular Biology Reports* 28:73-82.
[35].Koshwanez, J., Holl, M., Marquardt, B., Dragavon, J., Burgess, L., and Meldrum, D. 2004. Identification of budding yeast using a fiber-optic imaging bundle. *Rev. Sci. Instr*. 75:1363-1365.
[36].Kuznetsov A, Krn M, Kopell N,(2004/05) Synchrony in a population of hysteresis-based genetic oscillators. *SIAM J. Appl. Math*. 65:392-425
[37].Lord PG, Wheals AE (1980) Asymmetricaldivision of Saccharomyces cerevisiae. *J. Bacter*. 142:808-818.
[38].Lyon GJ, Novick RP (2004) Peptide signaling in Staphylococcus aureus and other Gram positive bacteria. *Peptides* 25:1389-1403.
[39].Lloyd AL, JVAA, (2004) Spatiotemporal dynamics of epidemics: synchrony in meta population models. Topics in biomathematics and related computational problems. *Math. Biosci*. 188:1-16.
[40].Mirollo RE, Strogatz SH, (1990) Synchronization of pulse-coupled biological oscillators. *SIAM J. Appl. Math*. 50:1645-1662.
[41].Muller D, Exler S, Aguilera-Vazquez L,Guerrero-Martin E, Reuss M (2003) Cyclic AMP mediates the cell cycle dynamics of energy metabolism in Saccharomyces cervisiae. *Yeast* 20:351-367.
[42].Munch T, Sonnleitner B, Fiechter A (1992) The decisive role of the Saccharomyces cervisiae cell cycle behavior for dynamic growth characterization. *J. Biotechnol*. 22:329 352.
[43].Murray D, Klevecz RR, Lloyd D (2003) Generation and maintenance of synchrony in Saccharomyces cerevisiae continuous culture. Experimental Cell Research 287:10-15.
[44].Palkova Z, Forstova J (2000) Yeast colonies synchronize their growth and development. *J. Cell Science* 113:1923-1928.

[45].Palkova Z, Vachova L (2006) Life within a community: benefits to yeast long term survival. FEMS. *Microbiol. Rev*. 30:806-824.
[46].Patnaik PR (2003) Oscillatory metabolism of Saccharomyces cerevisiae: An overview of mechanisms and models. *Biotechnology Advances* 21:183-192.
[47].Pikovsky A, Zaks M, Rosenblum M, Osipov G, Kurths J, (1997) Phase synchronization of chaotic oscillations in terms of periodic orbits. *Chaos* 7:680-687.
[48].Pringle JR, (1991)Staining of bud scars and other cell wall chitin with calcoflour. *Methods In Enzymology* 194:732-735.
[49].Richard P, (2003) The rythm of yeast. FEMS *Microbiol. Rev*. 27:547-557.
[50].Rotenberg M, (1977) Selective synchrony of cells ofdifferent cycletimes. *J. Theor. Biol*. 66:389-398.
[51].Rulkov NF, Afraimovich VS, (2003) Detectability of nondifferentiable generalized synchrony. *Phys. Rev. E* 67:066218
[52].Satroutdinov AD, Kuriyama H, Kobayashi H, (1992) Oscillatory metabolism of Saccharomyces cerevisiae in continuous culture. FEMS *Microbiology Lett*. 98:261-268.
[53].Singer RA, Johnston GC (1981) Nature of the G1 phase of the yeast Saccharomyces cerevisiae. *Proc. Natl. Acad. Sci* 78:3030-3033.
[54].Stowers C, Boczko EM (2010) Extending cell cycle synchrony and deconvolving population effects in budding yeast through an analysis of volume growth with a structured Leslie model. *JBiSE* 3:987-1001.
[55].Stowers C, Robertson JB, Ban H, Tanner RD, Boczko EM (2009) Periodic Fermentor Yield and Enhanced Product Enrichment from Autonomous Oscillations. Applied *Biochemistry and Biotechnology* 156:59.
[56].Strogatz SH, Mirollo RE, Matthews PC, (1992) Coupled nonlinear oscillators below the synchronization threshold: relaxation by generalized Landau damping. *Phys. Rev. Lett.* 68:2730-2733.
[57].J. Sun, C. Stowers, E.M. Boczko, and D. Li,(2010) Measurement of the Growth Rate of Individual Budding Yeast with Novel MOSFET-Based Microfluidic Coulter Counters. Lab-on-a-chip DOI:10.1039/C005029F.
[58].Terman D,(2001) Synchrony in networks of neuronal oscillators. Multiple-time-scale dynamical systems (Minneapolis, MN,1997), *IMA Vol. Math. Appl*. 122:215–232, Springer, New York, 2001.
[59].Tu BP, Kudlicki A, Rowicka M, McKnight SL (2005) Logic of the yeast metabolic cycle: temporal compartmentation of cellular processes. *Science* 310:1152-1158.
[60].Tvegard T, Soltani H, Skjolberg HC, Krohn M, Nilssen EA, et al.(2007) A novel checkpoint mechanism regulating the G1/S transition. *Genes and Development* 21:649-654.
[61].Von Meyenburg K (1973) Stable synchronous oscillations in continuous cultures of S. cerevisiae under glucose limitation. In B. Chance (Ed) Biological Biochemical Oscillators *Academic Press,* NY. 411.
[62].Walker G (1999) Synchronization of yeast cell populations. *Methods in Cell Science* 21:87 93.
[63].Wang J, Liu W, Uno T, Tonozuka H, Mitsui K, Tsurugi K (2000) Cellular stress response oscillate in synchronization with the ultridian oscillation of energy metabolism in the yeast Saccharomyces cervisiae. *FEMS Microbiol. Lett.* 189:9-13.
[64].Wolf J, Sohn H-Y, Heinrich R, Kuriyama H (2001) Mathematical analysis of a mechanism for autonomous oscillations in a continuous culture of Saccharomyces cerevisiae. *FEBS Lett*. 499:230-234.
[65].Woldringh CL, Huls PG, Vischer NOE (2003) Volume growth of daughter and parent cells during the cell cycle of Saccharomyces cerevisiae a/α as determined by image cytometry. *J. Bacteriology* 175:3174-3181.
[66].Xu Z, Tsurugi K (2006) A potential mechanism of energy metabolism oscillation in an aerobic chemostat culture of the yeast Saccharomyces cervisiae. *FEBS Journal* 273:16961709.
[67].Zhu G, Zamamiri A, Henson MA, Hjortsø MA (2000) Model predictive control of continuous yeast bioreactors using cell population balance models. Chemical Engineering *Science* 55:6155-6167.